CrystEngComm

Accepted Manuscript

ROYAL SOCIETY OF CHEMISTRY

www.rsc.org/crystengcomm

Mass-transport driven growth dynamics of AlGaAs shells deposited around dense GaAs nanowires by metalorganic vapor phase epitaxy

Ilio Miccoli,[†] *Paola Prete,*[‡,*] *and Nico Lovergine* [†]

[†] Dipartimento di Ingegneria dell'Innovazione, Università del Salento, Via Monteroni, I-73100 Lecce, Italy

[‡] Istituto per la Microelettronica e i Microsistemi, Consiglio Nazionale delle Ricerche, UOS Lecce, Via Monteroni, I-73100 Lecce, Italy

Abstract. III-V compound semiconductor nanowires with radial modulation of the materials composition and/or doping in the form of core-shell and core-multishell nanowire heterostructures promises novel and high-performance nano-scale light emitting diodes, lasers, photodetectors and solar cells. Strict control over the growth of such radially-heterostructured nanowires is however, necessary. We report on the experimental dependence of AlGaAs shell growth by metalorganic vapor phase epitaxy (MOVPE) around free-standing Au-catalysed GaAs nanowires on the nanostructure relevant size and densities. A model based on (i) the vapor mass-transport of group-III species, and (ii) perfect conformality

[*] Corresponding author (Paola Prete). e-mail: paola.prete@cnr.it ; phone: +39 0832 297 250; fax: +39 0832 297 249.

between nanowires and substrate of AlGaAs deposition is proposed and validated, describing the observed MOVPE growth dynamics of the shell material around dense ensembles of GaAs nanowires. We predict a complex (non-linear) dependence of the shell growth rate on initial GaAs nanowire diameters (ie., initial Au-catalyst nanoparticle size), heights, local densities on the substrate, and deposition time, in very good agreement with experimental data: in particular, a monotonic decrease of AlGaAs shell thickness is expected and observed with increasing the nanowire density.

Keywords: III-V semiconductors, core-shell nanowires, nanowire size, MOVPE, growth rate, vapor mass-transport, growth modelling.

I. INTRODUCTION

III-V compound semiconductors based nanowires have gathered considerable research interests in recent years as they are expected to impact several device technology fields, ranging from nanoelectronics[1], to nanophotonics[2,3], and photovoltaics[4,5] by offering both unprecedented materials properties[6], and novel device geometries[7] and functionalities[8].

Radial modulation of the nanowire composition and/or doping in the form of core-shell and core-multishell nanowire heterostructures leads to several materials/device advantages: among others, (i) radial p-n junctions in core-(multi)shell nanowires can greatly enlarge the junction area as compared to planar device counterparts having the same surface area, thus enhancing the performances of light emitting diodes, photodetectors and solar cells; (ii) the use of a larger band-gap semiconductor shell around III-V (especially GaAs) core nanowires has been shown effective in the suppression of the materials surface states, leading to enhanced radiative efficiency and increased carrier mobility and recombination lifetimes;[9,10,11] and (iii) suitable choices of the heterostructure materials band offsets and refractive indexes provide an effective way of radially confining carriers within the core, and may also improve the nanowire optical confinement leading to the observation of optical microcavity modes.[12]

The growth of core–shell nanowire heterostructures has been reported for a variety of III–V compound systems, including InAs-InP,[13] GaAs-GaInP,[14] GaAs-AlInP,[15] InAs-InAlAs[16] and GaAs-AlGaAs.[9,17,18] Recently, GaAs-AlGaAs core-multishell nanowires were also reported.[3] A common approach to the bottom-up synthesis of such nanostructures by metalorganic vapor phase epitaxy (MOVPE) is through the so-called Vapor-Liquid-Solid (VLS) mechanism using metal nanoparticles as catalyst for the self-assembly process of the nanowire core, followed by (multi)shell material overgrowth by conventional (Vapor-Solid) MOVPE.[13,14,18]

In order to exploit MOVPE technology for the fabrication of core-shell nanowire based devices, strict control over the growth process of radially-heterostructured nanowires is necessary. While much efforts have been devoted in the literature to understanding/modelling the VLS growth of III-V nanowires,[19] studies on shell materials have focussed until now on their inner composition/structure,[20,21] or on the effects of MOVPE process parameters (e.g., temperature, V:III molar ratio in the vapor) on electronic/radiative properties of resulting core-shell heterostructures.[9-11] Less is known instead, on actual shell growth dynamics around free-standing core nanowires; in particular, the dependence of vapor-solid growth of a shell material on nanowire size and densities has never been considered before. In this work, a detailed analysis of AlGaAs shell growth in the MOVPE self-assembly of GaAs/AlGaAs core-shell nanowires is reported, demonstrating that the nanowire size (e.g. their diameter, height) and their local surface density on the substrate couple with the vapor mass-transport supply of III-group species to determine the actual shell growth rate and its dependence on MOVPE parameters.

II. EXPERIMENTAL

Free-standing GaAs-$Al_xGa_{1-x}As$ (x=0.33) core-shell nanowires were grown on either semi-insulating (111)B-GaAs wafers or heterostructured GaAs/(111)Si substrates by low (50 mbar) pressure metalorganic vapor phase epitaxy (MOVPE) in an Aixtron RD200 reactor. Trimethyl-gallium (Me_3Ga), trimethyl-aluminum (Me_3Al) and tertiarybutyl-arsine ($^tBuAsH_2$) were used as gallium, aluminium and arsenic precursors, respectively. The heterostructured GaAs/(111)Si substrates were synthesized by depositing at 400°C, and subsequently annealing at 730°C a relatively thin (40÷50 nm) and smooth GaAs epilayer on either exactly (111)-oriented or 4°-miscut (towards a $\langle 11\bar{2} \rangle$ direction) Si wafers following the procedures reported in Ref. 22.

Vertically aligned (yield>99%) and almost untapered GaAs nanowires with lengths in the 1–3 μm range were then synthesized at 400°C on the freshly-etched (111)B-GaAs substrates and as-grown GaAs/(111)Si samples by the so-called Vapor-Liquid-Solid (VLS) self-assembly process using mono-dispersed colloidal Au nanoparticles as catalysts. The nanoparticles were deposited on the substrates as described elsewhere,[23] achieving surface densities between 10^7 and 10^9 cm^{-2}. Once the growth of the GaAs nanowire cores was terminated the substrate temperature was increased up to 650°C under H_2+^{t}BuAsH_2 for the AlGaAs shell overgrowth by conventional MOVPE.

A fixed Me_3Ga molar flow rate of 12.2 μmol/min (corresponding to a Ga molar fraction of ~4.3×10^{-5}) was employed in the vapor phase for both core and shell growth, whereas the nominal Al molar fraction in the vapor x_v=[Me_3Al]/([Me_3Al]+[Me_3Ga]) during AlGaAs growth was kept constant at around x_v=0.5. The ^{t}BuAsH_2 molar flow rate during GaAs and AlGaAs growth for the samples in this study varied, corresponding to precursors V:III molar ratio in the vapor between 5:1 and 20:1. The shell growth time was 4 min or 10 min.

The nanowire morphology and dimensions were studied through field emission scanning electron microscopy (FE-SEM) observations, using a Zeiss microscope, equipped with a high resolution FE-SEM Gemini electron column. A primary electron beam acceleration voltage of 5 kV and a working distance of around 5 mm were employed, ensuring a FE-SEM lateral spatial resolution of ~2-3 nm.

III. RESULTS AND DISCUSSION

Figure 1(a-d) shows the morphology of as-grown GaAs-AlGaAs core–shell nanowires on both (111)B-GaAs (Fig. 1(a,b)) and heterostructured GaAs/(111)Si substrates (Fig. 1(c,d)). The nanowires appear as straight (kink-free) segments with their major dimension running normal to the substrate surface. Also, their diameters remain constant throughout their entire lengths, but for a small tapered section close-by their upper end, where the original Au

nanoparticle (used to grow the GaAs core) is still clearly visible. Furthermore, the nanowires show hexagonal cross-sections, their six sidewall facets being normal to one of the three equivalent in-plane ⟨110⟩ substrate directions.[18] However, different (average) diameter values are clearly observed for the nanowire ensembles imaged in Fig. 1(a,d).

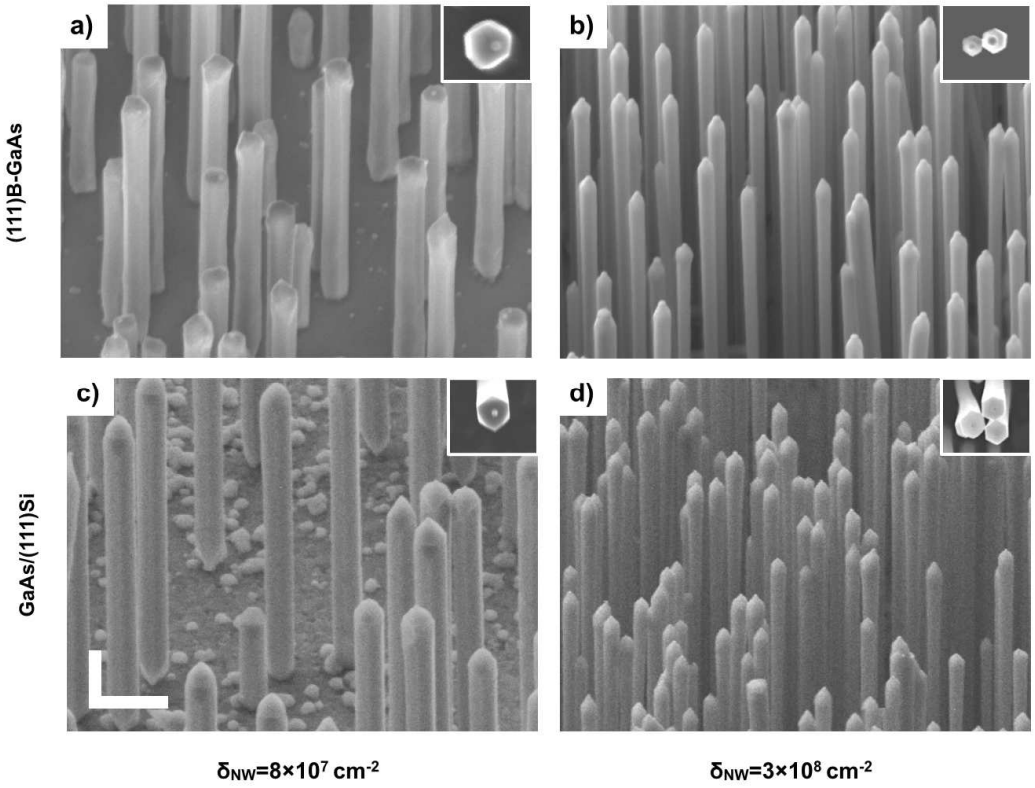

Figure 1. FE-SEM micrographs (45° tilt-view) of GaAs-AlGaAs core-shell nanowires grown on (a,b) (111)B-GaAs and (c,d) 4°-miscut GaAs/(111)Si heterosubstrates, corresponding to a nanowire surface density (δ_{NW}) of 8×10^7 cm^{-2} (a,c), and 3×10^8 cm^{-2} (b,d). The micrographs belong to different areas of the same samples. For all samples the AlGaAs shell growth time was 10 min. Insets in (a-d) are magnified plan-view micrographs of single/few GaAs-AlGaAs core-shell nanowires selected from areas corresponding to the larger images. White markers in the micrographs represent 1 μm.

Since the catalyst Au nanoparticles were deposited by dropping a small amount of the aqueous colloidal solution directly onto the substrate, the nanowire density turns rather

inhomogeneous across the substrate surface and can vary even more from sample to sample. FE-SEM micrographs in Fig. 1 were recorded at selected positions across two samples, where different nanowire surface densities occurred, suggesting that the core-shell diameters decrease with increasing the nanowire density.

A quantitative (and more statistically sound) confirmation of this phenomenon was obtained through the analysis of recorded FE-SEM plan-view images, which allowed estimating for each nanostructure in the micrographs the average GaAs core diameter and the corresponding AlGaAs shell thickness. As our initial GaAs core nanowires do show a negligible (within the FE-SEM spatial resolution limits) degree of tapering,[24] their diameter almost coincides with that (D_{Core}) at the nanowire tip, which in turn relates to the diameter (D_{Au}) of the Au nanoparticle from which the nanowire self-assembled: in the VLS process D_{Core} and D_{Au} are in fact connected through the relationship

$$D_{Core} = D_{Au} \cdot \sin\beta \qquad (1)$$

where β is the contact-angle formed at the triple-phase line of the Au droplet, the GaAs nanowire and the vapor; experimentally $90° \leq \beta \leq 127°$ after growth,[25,26] with a preference for higher contact angles ($\beta \cong 125° - 127°$) for GaAs nanowires in the zincblend (ZB) phase. As our GaAs nanowires exhibit pure ZB phase,[27] we set $\sin\beta = 0.81$ in Eq. (1).

Figs. 2(a) and 2(c) report the count histograms of the core-shell nanowire diameters D_{NW}, taken as the diagonal length of the nanowire hexagonal section normal to the (110) facets - Fig. 2(d)] and those (D_{Au}) of the Au nanoparticles at their tips, as measured from a series of plan-view micrographs, for a sample similar to that in Fig. 1(a,b). It must be noted here that the above FE-SEM analysis, refers to a limited surface area of the sample ($\sim$100 μm^2), where the density of core-shell nanowires remains fairly constant (within a 10% around $\delta_{NW} = 7 \times 10^8$ cm^{-2}). Both distributions in Figs. 2(a,c) can be best-fitted by the Γ-distribution function[28]:

$$P_{D_0,M}(D) = \frac{1}{\Gamma(M)}\left(\frac{M}{D_0}\right)^M \cdot \exp\left(-\frac{M}{D_0}D\right)D^{M-1} \qquad (2)$$

where D_0 is the average nanoparticle (nanowire) diameter, M is the distribution shape parameter and Γ is Euler's function. Best-fitting the count histogram in Fig. 2(a) with Eq. (2) returns an Au nanoparticle average diameter D_0^{Au} =55.0±0.8 nm and a shape parameter M=24.9±3.7, leading to a distribution standard deviation $\delta D_{Au} = D_0^{Au}/\sqrt{M}$ =11.0 nm (20.0%

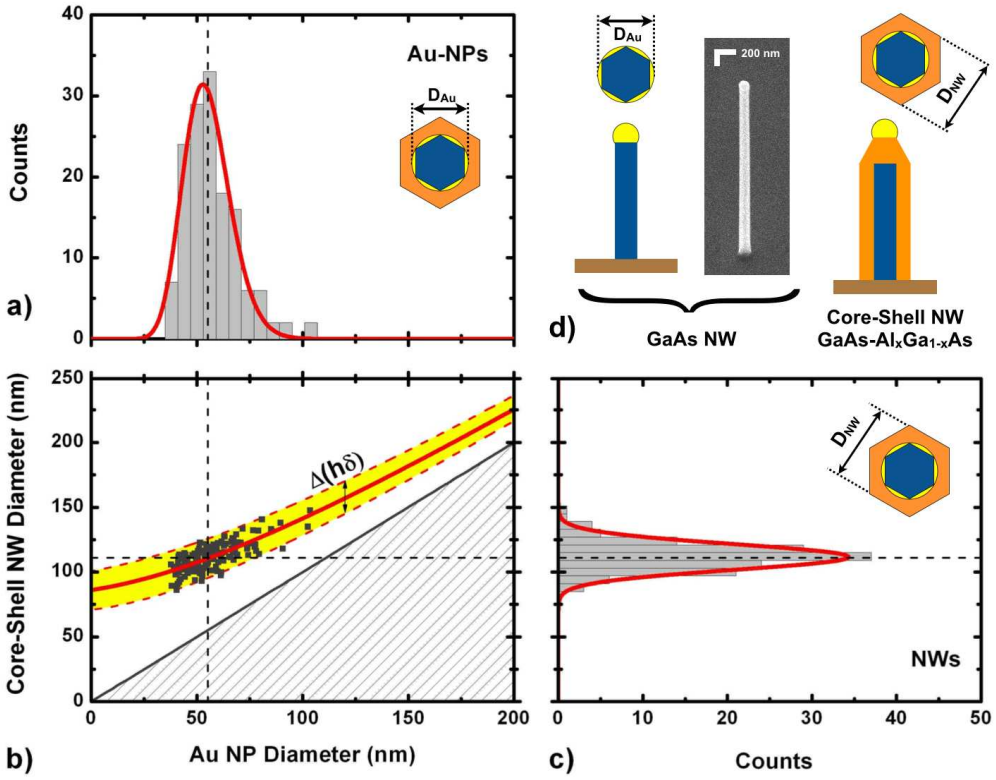

Figure 2. Count histograms of (a) Au nanoparticle diameters (D_{Au}) at the tips of GaAs-AlGaAs core-shell nanowires, and (c) corresponding nanowire diameters (D_{NW}) measured normal to the nanowire facets [schematics in (d)]. Solid curves in (a),(c) represent the Γ-distribution function (Eq. (2)) best fitting the experimental data. (b) D_{NW} values (■) as function of D_{Au} for the selected ensemble of core-shell nanowires, while the solid line is their best-fit with Eq. (6). The shaded (yellow) band around the best-fitting curve represents the parameter variation $\Delta(h_{NW}\delta_{NW})$ necessary to account for the cloud of data points.

relative deviation). Similarly, from the count histogram in Fig. 2(c), we get a core-shell nanowire average diameter D_0^{NW} =111.6±0.6 nm and a standard deviation δD_{NW}=19.8 nm (17.7% relative deviation). Hence, assuming that the Au nanoparticle diameters do not appreciably change upon AlGaAs shell overgrowth, the average shell thickness h_0^{AlGaAs} of as-grown core-shell nanowires within the selected sample area can then be estimated as $h_0^{AlGaAs} = \left(D_0^{NW} - D_0^{Au} \cdot \sin\beta\right)/2$ =33.5±1.4 nm.

Similar analyses performed on various FE-SEM plan-view images demonstrated that while D_0^{Au} remains almost constant (around 60±5 nm) for all samples, the diameter of as-grown core-shell nanowires depends indeed on their local surface density. Fig. 3(a) shows the as-estimated core-shell nanowire average diameter D_0^{NW} as function of their local surface density, for several samples grown on the two different substrates (i.e. freshly-etched (111)B-GaAs substrates and GaAs/(111)Si samples) and over a wider range of nanowire local densities (i.e. between 10^7 cm^{-2} and 10^9 cm^{-2}). The experimental data in Fig. 3(a) can be subdivided into two distinct subsets, corresponding to core-shell nanowires with the AlGaAs shells grown for (I) Δt^{shell}=10 min, or (II) Δt^{shell}=4 min, and all samples were grown using the same molar flow rate of group-III species.

Fig. 3(a) demonstrates that the nanowire D_0^{NW} (or equivalently, their shell thickness and average growth rate) decreases rapidly for density values increasing between 1×10^7 cm^{-2} and 3×10^8 cm^{-2}, while a smoother dependence is shown for nanowire densities in the $3–12\times10^8$ cm^{-2} interval. In addition, the AlGaAs shell growth rate does not depend on the type of substrate used.

We herewith propose a mass-transport limited model of the shell growth that explains the observed trends. Since the AlGaAs growth around GaAs core nanowires is carried out at high

temperature (650°C), its growth process is known to be limited by the vapor mass-transport of group-III species.[29, 30] The growth rate of a planar AlGaAs epilayer can be thus written as:

$$R_{2D}^{0} = V_{AlGaAs} \cdot J_0 \quad (3)$$

where V_{AlGaAs} is the molar volume of the AlGaAs crystal, while J_0 is the molar flux rate of

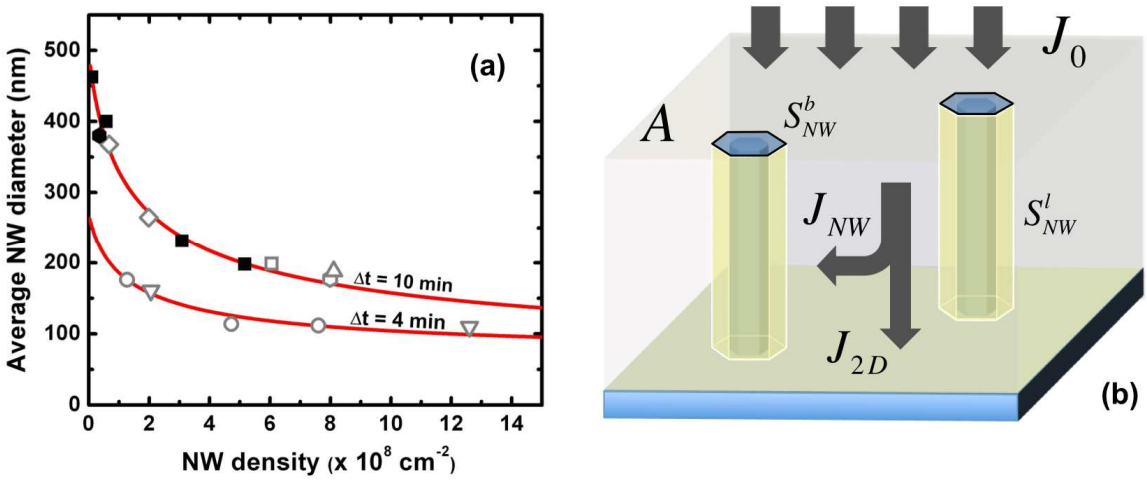

Figure 3. (a) Core-shell nanowire average diameter as function of the local nanowire surface density for two series of samples, whose AlGaAs shell was grown for (I) Δt^{shell}=10 min (■,□,⬢,△,◇) and (II) Δt^{shell}=4 min (○,▽). Open (full) symbols refer to core-shell nanowires grown onto freshly-etched (111)B-GaAs (GaAs/(111)Si hetero-) substrates. Solid curves represent the best-fit of experimental datasets I and II with Eq. (6). (b) Schematics showing the contribution of the impinging group-III molar flux rate (J_0) to planar (J_{2D}) and nanowire sidewall (J_{NW}) deposition of AlGaAs, along with geometrical quantities used in Eq. (4): i.e., the nanowire lateral ($S_{NW,i}^{l}$, yellow) and cross-sectional ($S_{NW,i}^{b}$, blue) areas.

group-III (Ga, Al) species reaching the growth surface. In the presence of free-standing nanowires, the same flux J_0 reaching the substrate must divide between the substrate free-surface and the total (i.e., summed over all (110)-facets) lateral surface of nanowires [see Fig. 3(b)]; the law of mass conservation allows then to write:

$$J_0 \cdot A = J_{NW} \cdot \sum_i S^l_{NW,i} \cdot n_{NW,i} + J_{2D} \cdot \left(A - \sum_i S^b_{NW,i} \cdot n_{NW,i} \right) \quad (4)$$

where A is the unit-surface area parallel to the substrate surface, $n_{NW,i}$ is the number of nanowires lying on the surface area A having lateral and cross-sectional areas given by $S^l_{NW,i}$ and $S^b_{NW,i}$, respectively, and the summations in Eq. (4) are performed over all possible nanowire geometric parameters (size), according to their experimentally observed distributions; finally, J_{NW} and J_{2D} are the (averaged over the local nanowire ensemble) III-group molar fluxes contributing to AlGaAs deposition around nanowires (shell growth) and on the substrate (planar growth), respectively. Under the additional hypothesis of (i) perfectly conformal growth (i.e. $J_{NW}=J_{2D}$), and (ii) that the nanowire diameter-to-height ratios (D_{NW}/h_{NW}) is very small, one is lead to write a differential equation for the time evolution of core-shell nanowire diameters given by (see Appendix)

$$\frac{dD_{NW}}{dt} \approx \frac{2R^0_{2D}}{1 + 2\sqrt{3} D_{NW} h_{NW} \delta_{NW}} \quad (5)$$

where δ_{NW} is the local nanowire density on the substrate surface. Eq. (5) describes the shell growth dynamics for an ensemble of dense free-standing nanowires under group-III mass-transport limited conditions. It predicts that the shell radial growth rate $R_{\mathrm{Shell}}=\frac{1}{2} dD_{\mathrm{NW}}/dt$ in the ⟨110⟩ direction decreases monotonically with increasing the core-shell nanowire diameters, and further it is inversely proportional to the local nanowire density and height. By integrating Eq. (5) over the time one obtains an analytic expression for the core-shell nanowire diameter D_{NW} as function of the shell growth time Δt^{shell}, and the nanowire density δ_{NW} and height h_{NW}:

$$D_{NW}\left(h_{nw}, D^0_{NW}, \delta_{NW}, \Delta t^{Shell}\right) = \frac{\sqrt{\left(1 + k\, h_{NW} \delta_{NW} D_{Core}\right)^2 + 4k\, h_{NW} \delta_{NW} R^0_{2D} \Delta t^{Shell}} - 1}{k\, h_{NW} \delta_{NW}} \quad (6)$$

where $k=2(3)^{1/2}$.

Eq. (6) has been used to best-fit the two datasets (I: Δt^{Shell}=10 min, and II: Δt^{Shell}=4 min) in Fig. 3(a): after imposing $D_{Core} = D_0^{Au} \cdot \sin\beta$ (and $D_0^{Au} \approx$60 nm), we then obtained for the remaining parameters in Eq (6): (I) h_{NW}=(924±165) nm, R_{2D}^0=(0.34±0.02) nm/sec for Δt^{Shell}=10 min (best-fit regression parameter *r=0.986*); and (II) h_{NW}=(1594±985) nm, R_{2D}^0=(0.35±0.12) nm/sec for Δt^{Shell}=4 min (best-fit regression parameter *r=0.964*). Strikingly, the AlGaAs planar growth rate R_{2D}^0 obtained from both best-fits coincides (within fitting errors) with that (R_{2D}^{exp}=0.33±0.03 nm/sec) measured for growth of relatively thick AlGaAs epilayers under identical MOVPE conditions. Noteworthy, the best-fitting value of h_{NW} obtained for dataset I is also in very good agreement (within fitting errors) with the nanowire heights (~1 μm) estimated from the FE-SEM images of the dataset samples. A higher uncertainty and larger discrepancy between best-fitted and measured (~3 μm) nanowire heights is observed instead for dataset II, although this may be ascribed to the lack of data points in the low ($\delta_{NW}<10^7$ cm^{-2}) density range, where a higher sensitivity to the actual (average) height of nanowires occurs in the least-square regression of Eq. (6).

Fig. 4 reports the calculated – based on Eq. (6) – values of D_{NW} on shell growth time (Δt^{Shell}), and Au nanoparticle diameter (D_{Au}) used as catalyst for the VLS growth of the GaAs nanowires for three different values of δ_{NW}. In Fig. 4(a) the $(\Delta t^{Shell})^{1/2}$ dependence of D_{NW} in Eq. (6) is more evident at low nanowire densities and long deposition times. Fig. 4(b) shows instead, how the size of the Au catalyst influences the final core-shell diameter D_{NW} [the $D_{NW}=D_{Au}$ solid line in the Figure delimits the area inaccessible to FE-SEM analysis]. Noteworthy is that for D_{Au} below ~25 nm, the slope of the D_{NW} vs D_{Au} curves tends to zero, and the effect of a broad distribution of the Au nanoparticle size becomes negligible.

The dependence shown in Fig. 4(b) was verified by best-fitting with Eq. (6) the cloud of data points reported in Fig. 2(b). In this case, fixing Δt^{Shell} and δ_{NW} values at 4 min and 7×10^8

cm^{-2} respectively, returned h_{NW}=(1327±860) nm and R_{2D}^{0} =(0.38±0.18) nm/sec as best-fitting parameters, in good agreement with previous estimates, further confirming the

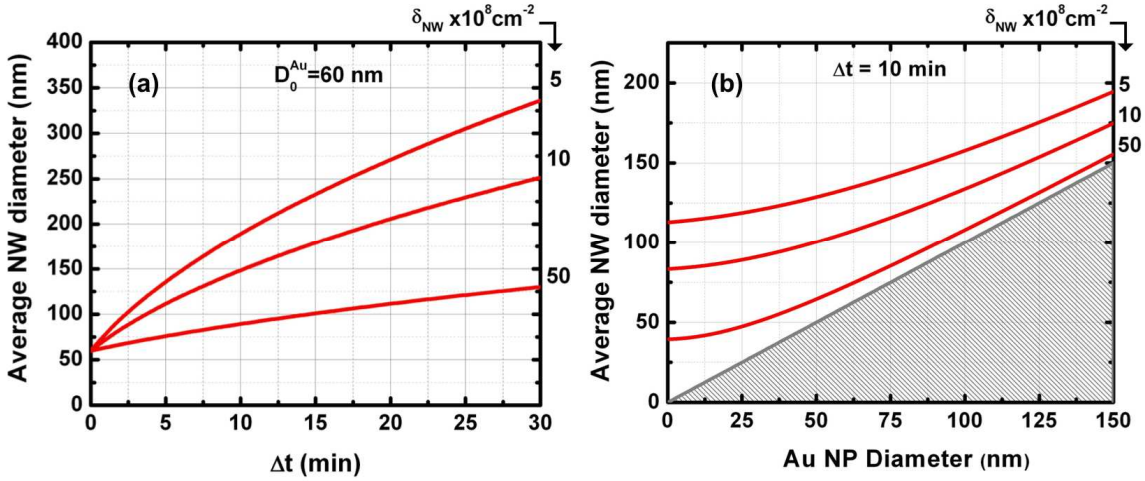

Figure 4. Values of the core-shell nanowire diameters D_{NW}, calculated from Eqs. (6) and (1) (and sinβ≅0.81), as function of (a) shell growth time Δt^{Shell} (taking D_0^{Au} =60 nm), and (b) Au nanoparticle diameter (for Δt^{Shell}=10 min), and for different nanowire densities δ_{NW} (values indicated in the diagrams).

validity of the model. We further notice that the cloud of measured D_{NW} values in Fig. 2(b) appears scattered around the best-fitting curve (i.e., for a fixed Au-catalyst diameter the AlGaAs shell thickness may show slightly different values) within a band accounted for by a parameter relative variation $\Delta(h_{NW}\delta_{NW})/h_{NW}\delta_{NW}$ ≈50%. Interestingly, FE-SEM micrographs used to obtain the data in Fig. 2(b) did show slight fluctuations in both the nanowire height ($\Delta h_{NW}/h_{NW}$≈30%) and local density ($\Delta\delta_{NW}/\delta_{NW}$≈10%), whose sum accounts for most of the above value.

CONCLUSIONS

We reported on experimental evidences of the dependence of AlGaAs shell deposition around free-standing GaAs nanowires on the nanostructure size and surface densities on the sample. A vapor mass-transport model was proposed, describing the MOVPE growth dynamics of the shell material around ensembles of GaAs nanowires, and validated by means of a detailed quantitative analysis of the nanostructure relevant size (diameters and heights of as-grown core-shell nanowires, Au-catalyst nanoparticle size at their tips). The model predicts a complex (non-linear) dependence of the shell growth rate on initial GaAs core nanowire diameters, heights, substrate local densities, and deposition time, in very good agreement with experimental data: in particular, a monotonic decrease of AlGaAs shell thickness is expected and observed with increasing the nanowire density. Furthermore, the model implies a conformal growth of the material both around the nanowires and on the underlying substrate free-surface in between them. Present results constitute a significant step towards our understanding of the MOVPE growth dynamics of III-V compound materials around dense free-standing nanowire ensembles, and for the controlled fabrication of radially modulated (i.e., core-shell and core-multishell) nanowire heterostructures with stringent/predictable compositional/dopant profile characteristics.

ACKNOWLEDGMENTS

The authors wish to acknowledge A. Pedio for FE-SEM observations and F. Marzo for assistance to the growth experiments.

APPENDIX: *MATHEMATICAL DERIVATION OF THE DIFFERENTIAL EQUATION DESCRIBING THE SHELL GROWTH DYNAMICS*

Let suppose that an ensemble of vertically free-standing prismatic nanowires, all having height h_{NW} and different hexagonal cross-sections of diameter $D_{NW,i}$ (where the i index identifies the i-th nanowire in the ensemble), occurs on a substrate with density δ_{NW}; the nanowire lateral and cross-sectional areas are expressed, at any given time t during the shell growth, by $S^l_{NW,i} = 2\sqrt{3}h_{NW}D_{NW,i}$ and $S^b_{NW,i} = \left(\sqrt{3}/2\right)D^2_{NW,i}$ (see Fig. A1).

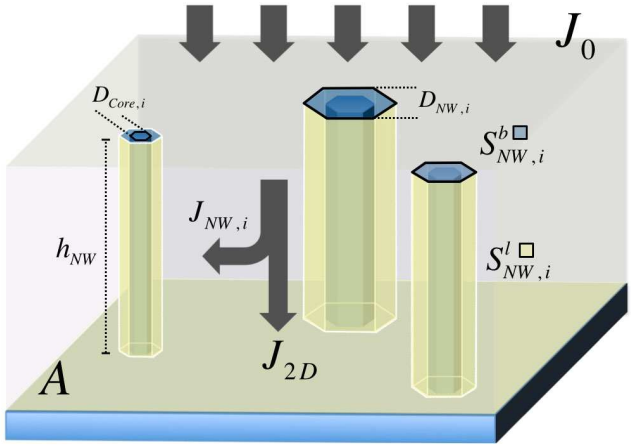

Figure A1. Schematics for the geometry of vertically free-standing nanowires on a substrate area A. The nanowire lateral and cross-sectional areas $S^l_{NW,i}$ and $S^b_{NW,i}$ are indicated in yellow and blue, respectively. $D_{Core,i}$ and $D_{NW,i}$ are the core diameter and the core-shell diameter of the *i*-th nanowire.

Application of the law of mass conservation to the III-group precursors molar flux rate J_0 reaching the nanowire ensemble from the vapor allows to write:

$$J_0 \cdot A = \sum_i J_{NW,i} \cdot S^l_{NW,i} \cdot n_{NW,i} + J_{2D} \cdot \left(A - \sum_i S^b_{NW,i} \cdot n_{NW,i} \right), \qquad \text{(A1)}$$

where $J_{NW,i}$ and J_{2D} are the III-group molar flux rates contributing to AlGaAs deposition on the sidewalls of each nanowire and on the substrate, respectively, A is the unit-surface area parallel to the substrate surface, $n_{NW,i}$ is the number of nanowires occurring on the surface of area A, and summations in Eq. (A1) are performed over all possible values of the nanowire diameter D. Values of $J_{NW,i}$ may depend on actual vapor conditions around each nanowire. We thus define the average flux rate

$$J_{NW} = \frac{\sum_i J_{NW,i} \cdot S^l_{NW,i} \cdot n_{NW,i}}{\sum_i S^l_{NW,i} \cdot n_{NW,i}} . \quad \text{(A2)}$$

If V_{AlGaAs} is the molar volume of the AlGaAs shell, the incremental volume change $d\tau_{NW,i}$ (for the *i-th* nanowire) due to the lateral shell overgrowth over the time interval dt can be calculated from

$$\frac{d\tau_{NW,i}}{dt} = V_{AlGaAs} \cdot J_{NW,i} \cdot S^l_{NW,i} ;$$

in writing the relationship above we assume a uniform V_{AlGaAs} value for the shell, in reason of the negligible change of V_{AlGaAs} with the Al-content.[31] Well-known compositional anisotropies occurring within the shell of both MBE- (Refs. 32,33) and MOVPE-grown[20,21] GaAs-$Al_xGa_{1-x}As$ core-shell nanowire samples cannot thus affect present calculations, and are neglected in the following.

The quantity in the numerator of Eq. (A2) can be then written

$$\sum_i J_{NW,i} \cdot S^l_{NW,i} \cdot n_{NW,i} = \frac{1}{V_{AlGaAs}} \sum_i \left(\frac{d\tau_{NW,i}}{dt} \right) \cdot n_{NW,i} \cong \frac{n_{NW}}{V_{AlGaAs}} \int_0^{+\infty} \left(\frac{d\tau_{NW}}{dt} \right) P_{D_0,M}(D_{NW}) dD_{NW} \quad \text{(A3)}$$

where in the last expression on the right we substituted the summation over all nanowire diameters with the integration over dD_{NW} and introduced the Γ-distribution function

$$P_{D_0^{NW},M}(D) = \frac{1}{\Gamma(M)} \left(\frac{M}{D_0^{NW}} \right)^M \cdot \exp\left(-\frac{M}{D_0^{NW}} D_{NW} \right) D_{NW}^{M-1}$$

describing the statistical distribution of nanowire diameters (D_0^{NW} being the average diameter, M the so-called shape parameter of the distribution, and Γ(M) is Euler's Gamma function);[23] furthermore, n_{NW} is the total number of nanowires over the area A [$dn_{NW}(D_{NW}) = P_{D_0^{NW},M}(D_{NW})dD_{NW}$ being thus the number of nanowires with diameter values comprised in the interval (D_{NW}, $D_{NW}+dD_{NW}$)]. Assuming that the nanowire height h_{NW} remains almost unchanged during the shell growth, the quantity $d\tau_{NW}/dt$ can be written

$$\frac{d\tau_{NW}}{dt} = \frac{d\left(h_{NW}S_{NW}^{b}\right)}{dD_{NW}} \cdot \frac{dD_{NW}}{dt} = \sqrt{3}h_{NW}D_{NW} \cdot \left(\frac{dD_{NW}}{dt}\right) = \frac{\sqrt{3}}{2}h_{NW}\frac{d}{dT}\left(D_{NW}^{2}\right)$$

where $h_{NW}S_{NW}^{b}$ is the nanowire volume. Substituting into Eq. (A3) gives

$$\sum_i J_{NW,i} \cdot S_{NW,i}^{l} \cdot n_{NW,i} \cong \frac{\sqrt{3}n_{NW}}{2V_{AlGaAs}} \int_0^{+\infty} \frac{d\left(D_{NW}^{2}\right)}{dt} P_{D_0^{NW},M}(D_{NW})dD_{NW} = \frac{\sqrt{3}n_{NW}}{2V_{AlGaAs}} \cdot \frac{d}{dt} \int_0^{+\infty} D_{NW}^{2} \cdot P_{D_0^{NW},M}(D_{NW})dD_{NW}$$

The latter integral in the equation can be readily evaluated,[34] and after a few algebraic calculations one obtains

$$\sum_i J_{NW,i} \cdot S_{NW,i}^{l} \cdot n_{NW,i} \cong \frac{\sqrt{3}n_{NW}}{V_{AlGaAs}} h_{NW} D_0^{NW} \frac{dD_0^{NW}}{dt} \cdot \frac{(M+1)(M+2)}{M^2}. \quad \text{(A4)}$$

Similarly, the quantity in the denominator of Eq. (A2) is calculated as

$$\sum_i S_{NW,i}^{l} \cdot n_{NW,i} \cong n_{NW} \int_0^{+\infty} S_{NW}^{l} \cdot P_{D_0^{NW},M}(D_{NW})dD_{NW} = 2\sqrt{3}n_{NW}h_{NW}D_0^{NW}\frac{M+1}{M}. \quad \text{(A5)}$$

Substituting Eqs. (A4) and (A5) in Eq. (A2) one finally obtains a relationship for the average shell growth rate

$$R_{AlGaAs} = \frac{1}{2}\left(\frac{dD_0^{NW}}{dt}\right) = \left(\frac{M+2}{M}\right)V_{AlGaAs}J_{NW} \approx V_{AlGaAs}J_{NW}, \quad \text{(A6)}$$

and the last expression on the right holds as $\frac{M+2}{M}=\left[1+2\left(\frac{\delta D^{NW}}{D_0^{NW}}\right)^2\right]\approx 1$ with a good approximation, due to the relatively narrow ($\delta D^{NW}/D_0^{NW}\leq 20\%$) diameter distribution of present nanowires.

Now, assuming a perfectly conformal growth (i.e. $J_{NW}=J_{2D}$), from Eqs. (A1) and (A2) one writes

$$J_{NW}=\frac{J_0}{1+\frac{1}{A}\cdot\sum_1\left(S^l_{NW,i}-S^b_{NW,i}\right)\cdot n_{NW,i}}\cong\frac{J_0}{1+\frac{n_{NW}}{A}\cdot\int_0^{+\infty}\left[S^l_{NW}\left(D_{NW}\right)-S^b_{NW}\left(D_{NW}\right)\right]P_{D_0^{NW},M}\left(D_{NW}\right)dD_{NW}}$$

where $\delta_{NW}=n_{NW}/A$ is the local (i.e., over the same sample area where J_{NW} is calculated) nanowire density; taking into account that $(1/4)(D_{NW}/h_{NW})<<1$ for all nanowires, the integral in the denominator of the right expression can be calculated as [34]

$$J_{NW}=\frac{J_0}{1+2\sqrt{3}h_{NW}D_0^{NW}\delta_{NW}\cdot(M+1)/M}\ . \tag{A7}$$

Substituting the latter result in Eq. (A6), and taking $(M+1)/M\approx 1$ for the same reason as before, we finally get

$$\frac{dD_0^{NW}}{dt}=\frac{2R_{2D}^0}{1+2\sqrt{3}h_{NW}D_0^{NW}\delta_{NW}} \tag{A8}$$

where $R_{2D}^0=V_{AlGaAs}\cdot J_0$ is the growth rate of a planar layer of the AlGaAs alloy under the same vapor conditions adopted for growing the shell. Eq. (A8) describes the growth dynamics of AlGaAs around a dense ensemble of core nanowires, and predicts a time-dependent shell growth rate, whose actual value also depends on the nanowire size and density. Eq. (A8) can be easily integrated over the shell growth time Δt^{Shell}: writing D_{NW} instead of D_0^{NW} in the Equation for simplicity of notation one writes

$$\int_{D_{NW}^0}^{D_{NW}} \left(1 + 2\sqrt{3} h_{NW} D_{NW} \delta_{NW}\right) dD_{NW} = 2R_{2D}^0 \int_0^{\Delta t^{Shell}} dt = 2R_{2D}^0 \Delta t^{Shell}$$

where D_{NW}^0 is the average diameter of initial (at t=0) core nanowires. From integration one gets the algebraic equation

$$\left(D_{NW} - D_{NW}^0\right) + \sqrt{3}\left[\left(D_{NW}\right)^2 - \left(D_{NW}^0\right)^2\right] = 2R_{2D}^0 \Delta t^{Shell}$$

whose solution is finally

$$D_{NW}\left(h_{nw}, D_{NW}^0, \delta_{NW}, \Delta t^{Shell}\right) = \frac{\sqrt{\left(1 + k\, h_{NW} \delta_{NW} D_{NW}^0\right)^2 + 4k\, h_{NW} \delta_{NW} R_{2D}^0 \Delta t^{Shell}} - 1}{k\, h_{NW} \delta_{NW}}$$

with $k=2(3)^{1/2}$.

References

[1] S. A. Dayeh, D. P. R. Aplin, X. T. Zhou, P. K. L. Yu, E. T. Yu, and D. L. Wang, *Small*, 2007, **3**, 326.

[2] B. Mayer, D. Rudolph, J. Schnell, S. Morkötter, J. Winnerl, J. Treu, K. Müller, G. Bracher, G. Abstreiter, G. Koblmüller, and J. J. Finley, *Nat. Comm.*, 2013, **4**, 2931.

[3] K. Tomioka, J. Motohisa, S. Hara, K. Hiruma, and T. Fukui, *Nano Lett.*, 2010, **10**, 1639.

[4] J. Wallentin, N. Anttu, D. Asoli, M. Huffman, I. Åberg, M. H. Magnusson, G. Siefer, P. Fuss-Kailuweit, F. Dimroth, B. Witzigmann, H. Q. Xu, L. Samuelson, K. Deppert, and M. T. Borgström, *Science*, 2013, **339**, 1057.

[5] P. Krogstrup, H. I. Jørgensen, M. Heiss, O. Demichel, J. V. Holm, M. Aagesen, J. Nygard, and A. Fontcuberta i Morral, *Nat. Photon.*, 2013, **7**, 306.

[6] J. Bolinsson, P. Caroff, B. Mandl, and K. A. Dick, *Nanotechnol.*, 2011, **22**, 265606.

[7] K. Tomioka, M. Yoshimura, and T. Fukui, *Nature*, 2012, **488**, 189.

[8] G. Chen, E. M. Gallo, O. D. Leaffer, T. McGuckin, P. Prete, N. Lovergine, and J. E. Spanier, *Phys. Rev. Lett.*, 2011, **107**, 156802.

[9] N. Jiang, P. Parkinson, Q. Gao, S. Breuer, H. H. Tan, J. Wong-Leung, and C. Jagadish, *Appl. Phys. Lett.*, 2012, **101**, 023111.

[10] P. Parkinson, H. J. Joyce, Q. Gao, H. H. Tan, X. Zhang, J. Zou, C. Jagadish, L. M. Herz, and M. B. Johnston, *Nano Lett.*, 2009, **9**, 3349.

[11] C.-C. Chiang, C.-Y. Chi, M. Yao, N. Huang, C.-C. Chen, J. Theiss, A. W. Bushmaker, S. LaLumondiere, T.-W. Yeh, M. L. Povinelli, C. Zhou, P. D. Dapkus, and S. B. Cronin, *Nano Lett.*, 2012, **12**, 4484.

[12] L. Yang, J. Motohisa, T. Fukui, L. X. Jia, L. Zhang, M. M. Geng, P. Chen, and Y. L. Liu, *Opt. Expr.*, 2009, **17**, 9337.

[13] J. M. W. Van Tilburg, R. E. Algra, W. G. G. Immink, M. Verheijen, E. P. A. M. Bakkers, and L. P. Kouwenhoven, *Semicond. Sci. Technol.*, 2010, **25**, 024011.

[14] N. Skold, L. S. Karlsson, M. W. Larsson, M. E. Pistol, W. Seifert, J. Tragardhand, L. Samuelson, *Nano Lett.*, 2005, **5**, 1943.

[15] A. C. E. Chia, M. Tirado, Y. Li, S. Zhao, Z. Mi, D. Comedi, and R. R. LaPierre, *J. Appl. Phys.*, 2012, **111**, 094319.

[16] K. Tomioka, K. I. T. Tanaka, J. Motohisa, S. Hara, K. Hiruma, and T. Fukui, *J. Mater. Res.*, 2011, **26**, 2127.

[17] J. Noborisaka, J. Motohisa, S. Hara, and T. Fukui, *Appl. Phys. Lett.*, 2005, **87**, 093109.

[18] P. Prete, F. Marzo, P. Paiano, N. Lovergine, G. Salviati, L. Lazzarini, and T. Sekiguchi, *J. Cryst. Growth*, 2008, **310**, 5114.

[19] J. Johansson, C. P. T. Svensson, T. Mårtensson, L. Samuelson, and W. Seifert, *J. Phys. Chem. B*, 2005, **109**, 13567.

[20] C. Zheng, J. Wong-Leung, Q. Gao, H. H. Tan, C. Jagadish, and J. Etheridge, *Nano Lett.*, 2013, **13**, 3742.

[21] A. Lubk, D. Wolf, P. Prete, N. Lovergine, T. Niermann, S. Sturm, and H. Lichte, *Phys. Rev. B*, 2014, **90**, 125404.

[22] I. Miccoli, P. Prete, F. Marzo, D. Cannoletta, and N. Lovergine, *Cryst. Res. Technol.*, 2011, **46**, 795.

[23] P. Paiano, P. Prete, N. Lovergine, and A. M. Mancini, *J. Appl. Phys.*, 2006, **100**, 094305.

[24] For present GaAs nanowires we measured a tapering factor (defined as the nanowire sidewall-to-axial growth rate ratio) of ≤1.5 nm/μm: given the present nanowire heights (1-3 μm), this leads to estimate an axial (between tip and base) variation of each nanowire diameter within 2-5 nm around the average, i.e. comparable to the resolution limits of the

FE-SEM microscope under instrumental conditions employed for present observations (see Sect. Experimental).

[25] F. Glas, J.-C. Harmand, and G. Patriarche, *Phys. Rev. Lett.*, 2007, **99**, 146101.

[26] B. J. O'Dowd, T. Wojtowicz, S. Rouvimov, X. Liu, R. Pimpinella, V. Kolkovsky, T. Wojciechowski, M. Zgirski, M. Dobrowolska, I. V. Shvets, and J. Furdyna, *J. Appl. Phys.*, 2014, **116**, 063509.

[27] P. Prete, I. Miccoli, F. Marzo, and N. Lovergine, *Phys. Status Sol. – RRL*, 2013, **7**, 874.

[28] O. Nagao, G. Harada, T. Sugawara, A. Sasaki, and Y. Ito, *Jap. J. Appl. Phys.*, 2004, **43**, 7742.

[29] H. Prakash, *Prog. Cryst. Growth Charact.*, 1986, **12**, 243.

[30] G. B. Stringfellow, *Organometallic Vapor-Phase Epitaxy: Theory and Practice*, 2nd ed. (Academic Press, San Diego, CA, 1998).

[31] S. Adachi, *J. Appl. Phys.*, 1985, **58**, R1.

[32] D. Rudolph, S Funk, M. Döblinger, S. Morkötter, S. Hertenberger, L. Schweickert, J. Becker, S. Matich, M. Bichler, D. Spirkoska, I. Zardo, J. Finley, G. Abstreiter, and G. Koblmüller, *Nano Lett.*, 2013, **13**, 1522.

[33] M. Heiss, Y. Fontana, A. Gustafsson, G. Wust, C. Magen, D. D. O'Regan, J. W. Luo, B. Ketterer, S. Conesa-Boj, A. V. Kuhlmann, J. Houel, E. Russo-Averchi, J. R. Morante, M. Cantoni, N. Marzari, J. Arbiol, A. Zunger, R. J. Warburton, and A. Fontcuberta i Morral, *Nat. Mater.*, 2013, **12**, 439.

[34] Based on Euler's Γ-function well-known property $\Gamma(z+1)=z\,\Gamma(z+1)$ [and Re(z)>0], it is easy to demonstrate that $\int_0^{+\infty} x^m e^{-ax} dx = a^{-(m+1)}\,\Gamma(m+1)$ (with $m,a>0$); from the latter

relationship it follows $\int_0^{+\infty} D_{NW}^m \cdot P_{D_0^{NW},M}(D_{NW}) dD_{NW} = \left(D_0^{NW}\right)^m \cdot \frac{(M+1)(M+2)\cdot\ldots\cdot(M+m)}{M^m}$

(and m>0).